Supplementary information files for Probing the enhanced methanol electrooxidation mechanism on platinum-metal oxide catalyst

Supplementary Information

Probing Enhancement of Methanol Electrooxidation mechanism on Platinum-Metal Oxide Catalyst

Ya-Wei Zhou, Ya-Feng Chen, Kun Jiang, Zhen Liu, Zi-Jie Mao, Wei-Yi Zhang, Wen-Feng Lin* and Wen-Bin Cai*

*Corresponding authors: W.F. Lin (w.lin@lboro.ac.uk) or W.-B. Cai (wbcai@fudan.edu.cn)

Table of Contents

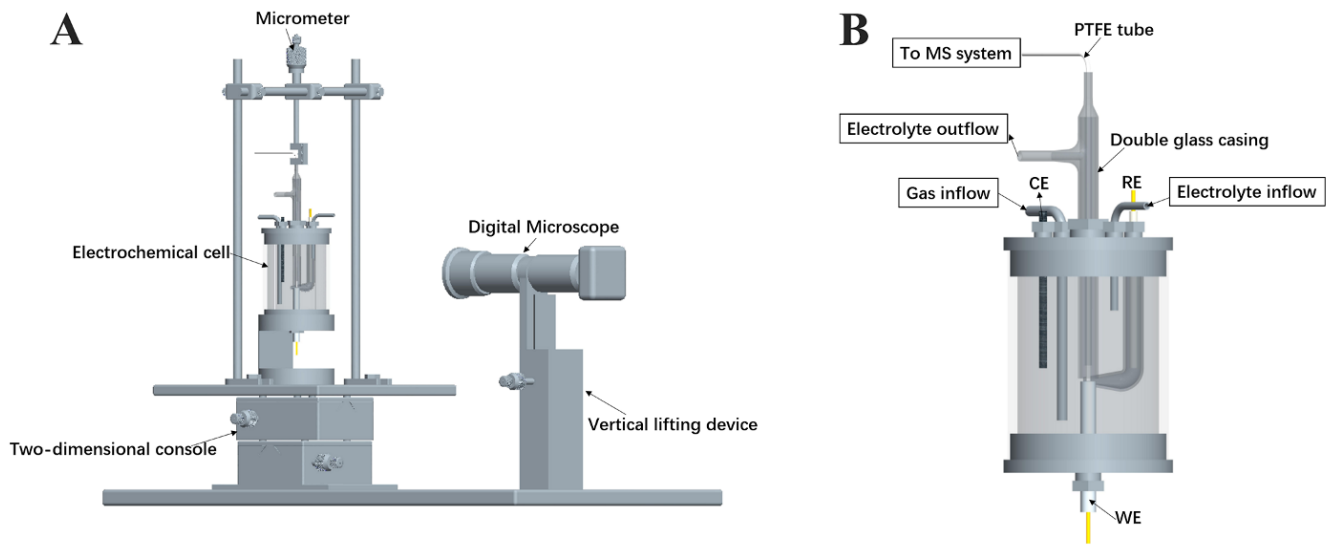

Figure S1. (A) Illustration of a new 'probe-type' on-line DEMS system; (B) Designing drawing of the on-line DEMS electrochemical cell.

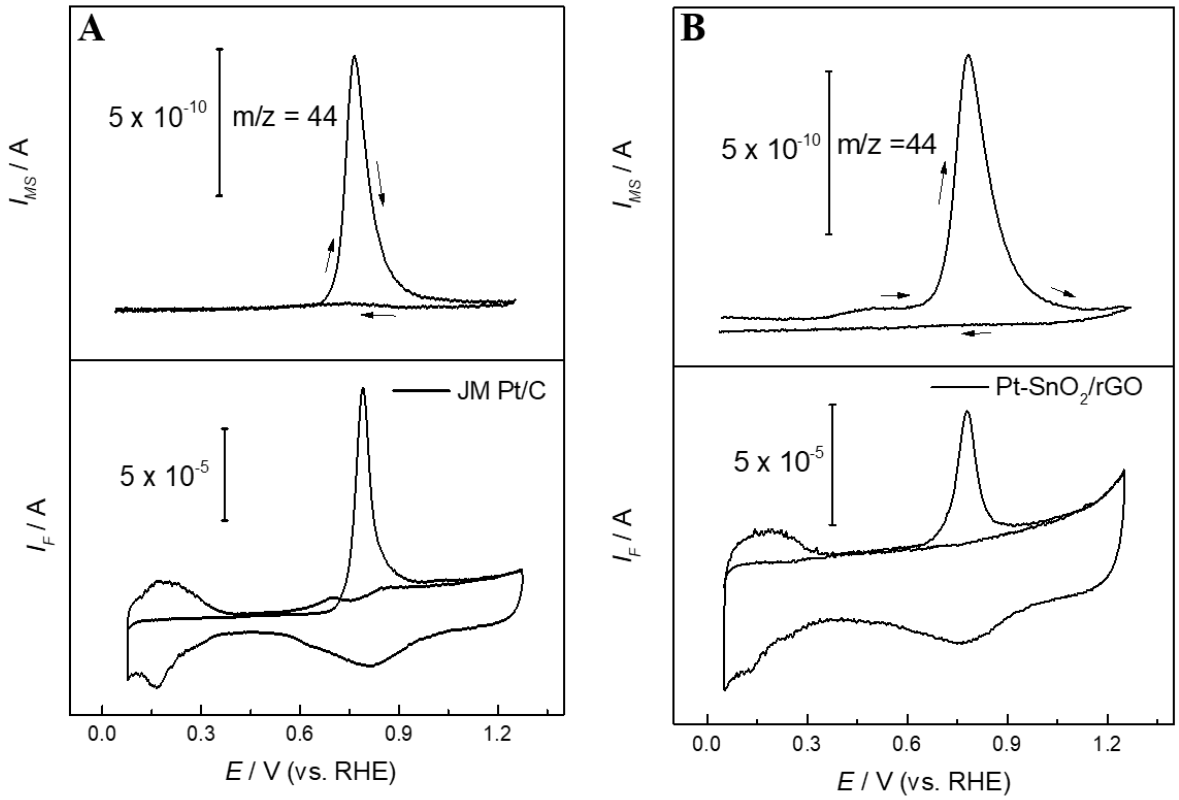

Figure S2. CO stripping curves of JM Pt/C (A) and Pt-SnO_2 /rGO (B), also shown are the corresponding MSCVs of CO_2 (m/z = 44)

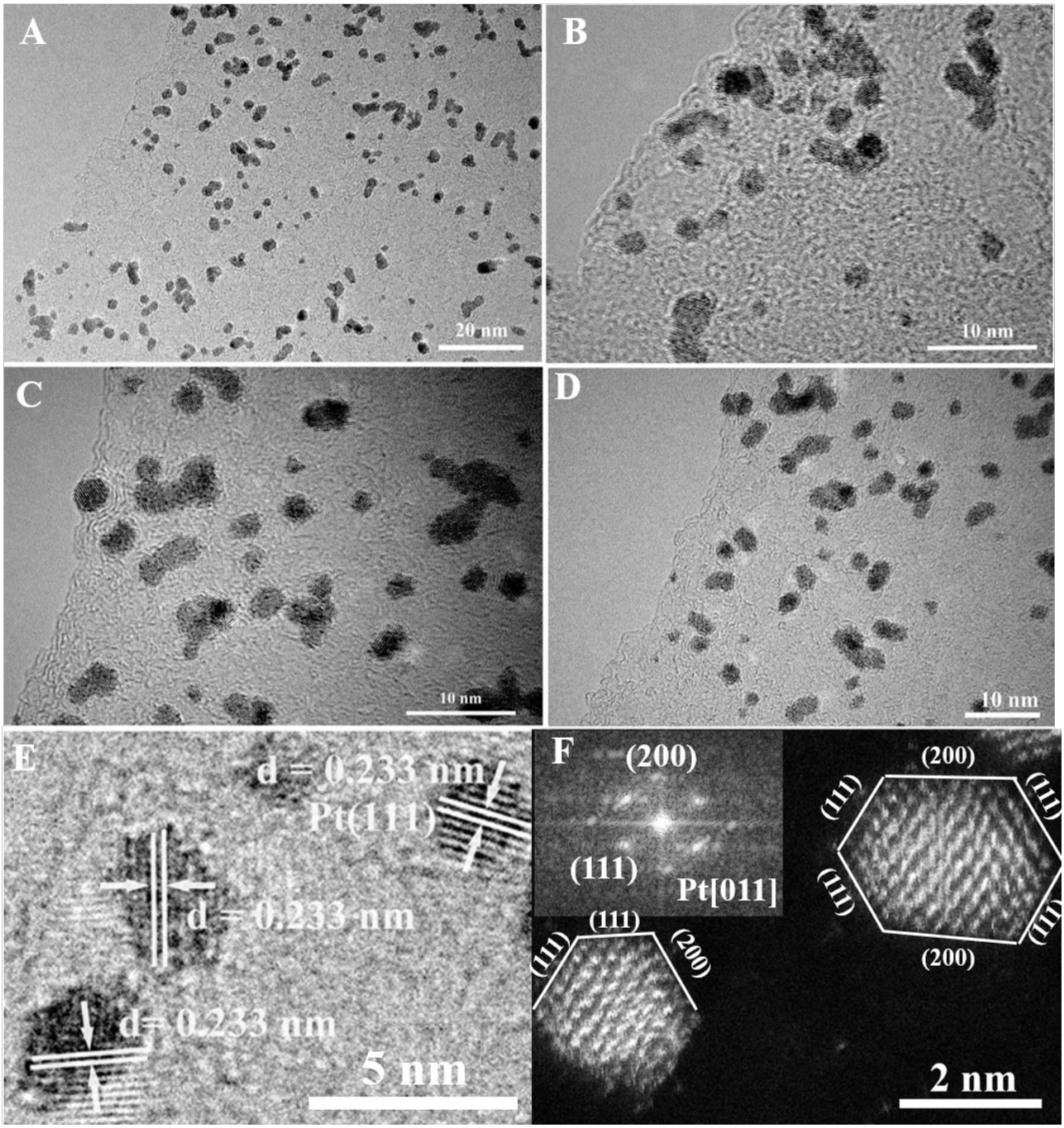

Figure S3. (A-D)TEM images of the as-prepared Pt-SnO_2 /rGO composites, (E) HR-TEM images of Pt-SnO_2 /rGO, (F) Atomically resolved HAADF-STEM image of Pt-SnO_2. Left inset is the FFT of the image (F). From the HR-TEM images, the lattice distance of Pt overlayer on SnO_2 was found to be 2.33 Å. This is slightly larger than that of the Pt (111) (2.26 Å), which could be ascribed to the tensile strain effect from the SnO_2 substrate. The Pt-SnO_2 nanoflakes in HAADF-STEM image (Figure S1F) were founded to be oriented along the [011] direction with (111) and(002) facets being the abundant truncating lattice planes, which were further confirmed by the corresponding fast Fourier transform image.

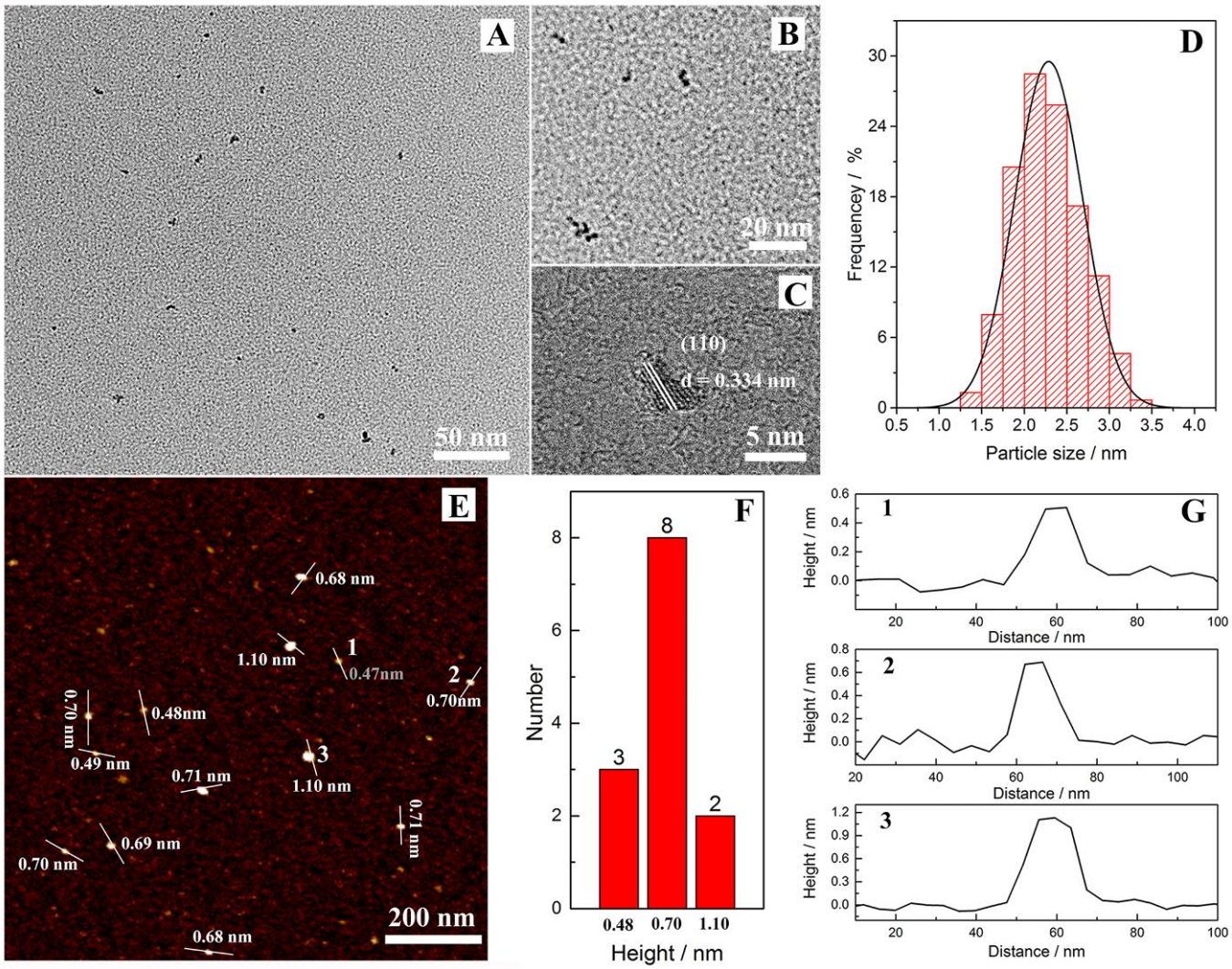

Figure S4. SnO_2 nanoslices characterization. (A-C) Bright field (HR-)TEM images, (D) size distribution, (E) AFM image with marked white line and number showing the height of certain SnO_2 nanoslices, (F) corresponding height distribution and (G) height profiles.

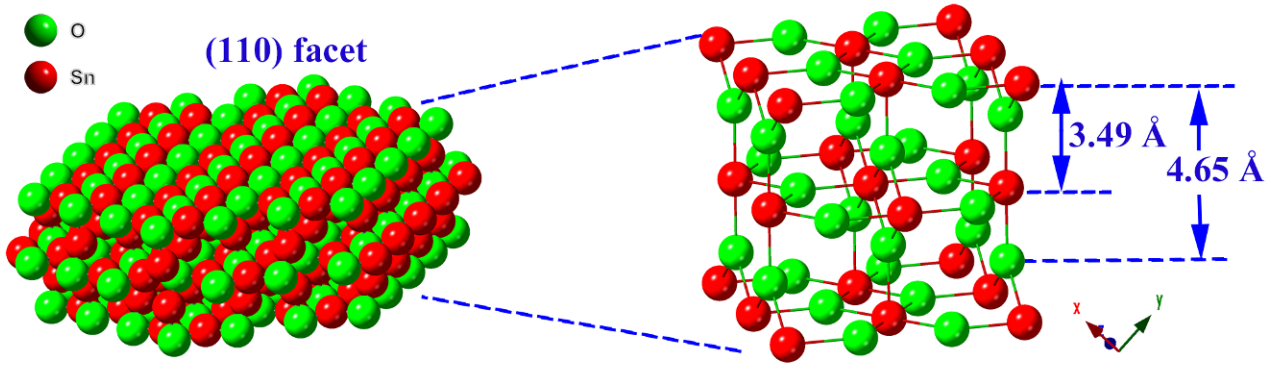

Figure S5. Schematic illustration of ultrathin SnO_2 nanoslices.

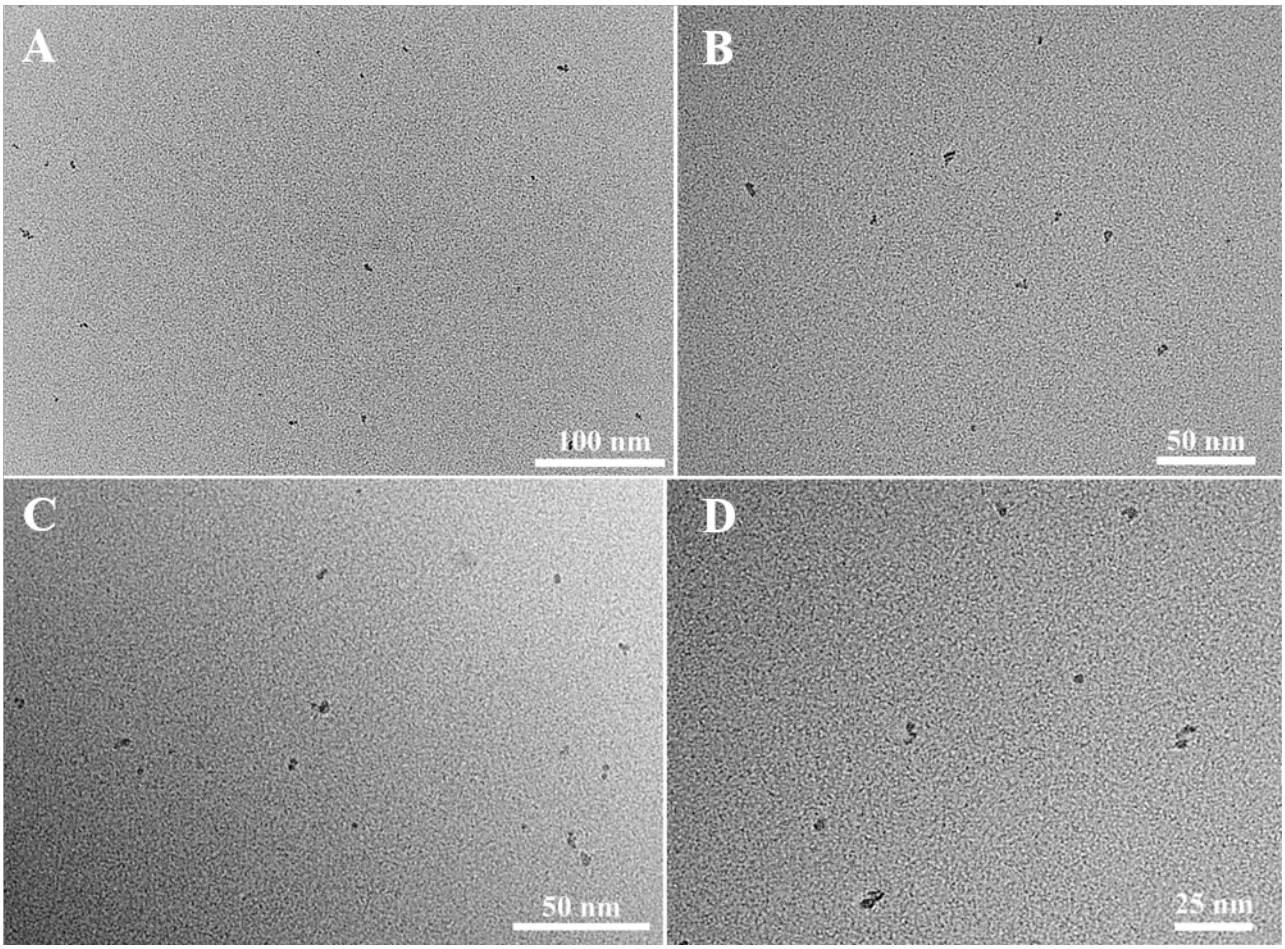

Figure S6. Additional TEM images of SnO_2 nanoslices.

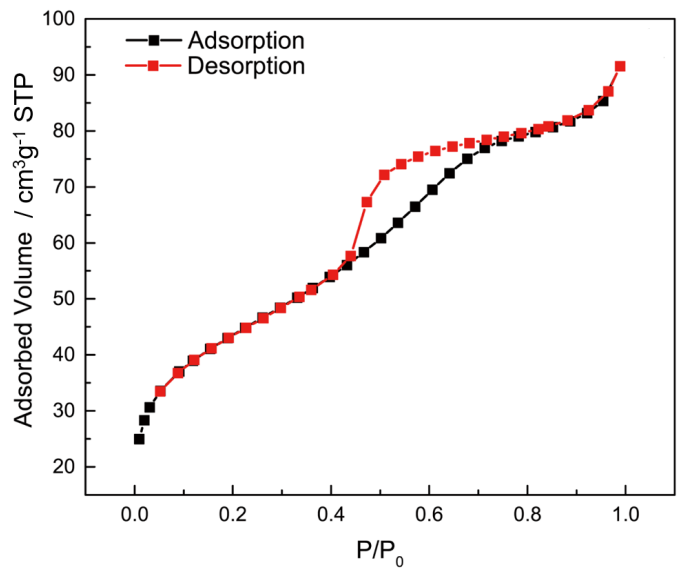

Figure S7. N_2 sorption isotherms of ultrathin SnO_2 nanoslices. The special surface area of ultrathin SnO_2 nanoslices was estimated to be about 151.95 m^2 g^{-1} from the N_2 sorption isotherms.

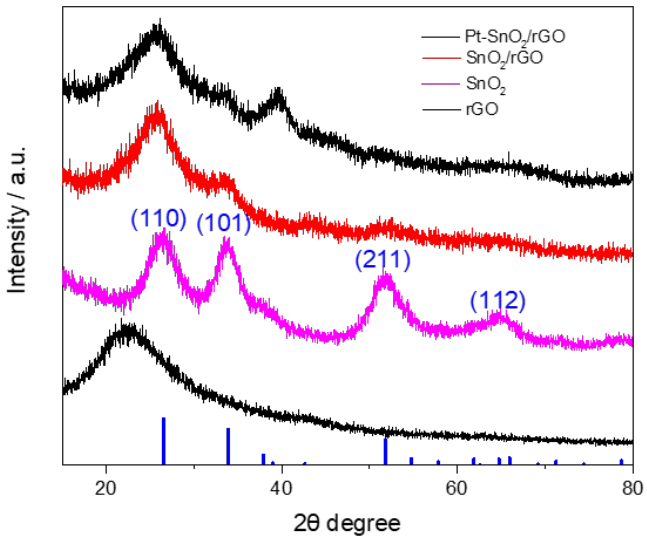

Figure S8. XRD patterns of reduced graphene oxide (rGO), SnO_2 powder, SnO_2/rGO and Pt-SnO_2/rGO composites. The bule lines are indexed to the tetragonal structure of SnO_2, corresponding to JCPDS No. 88-0287.

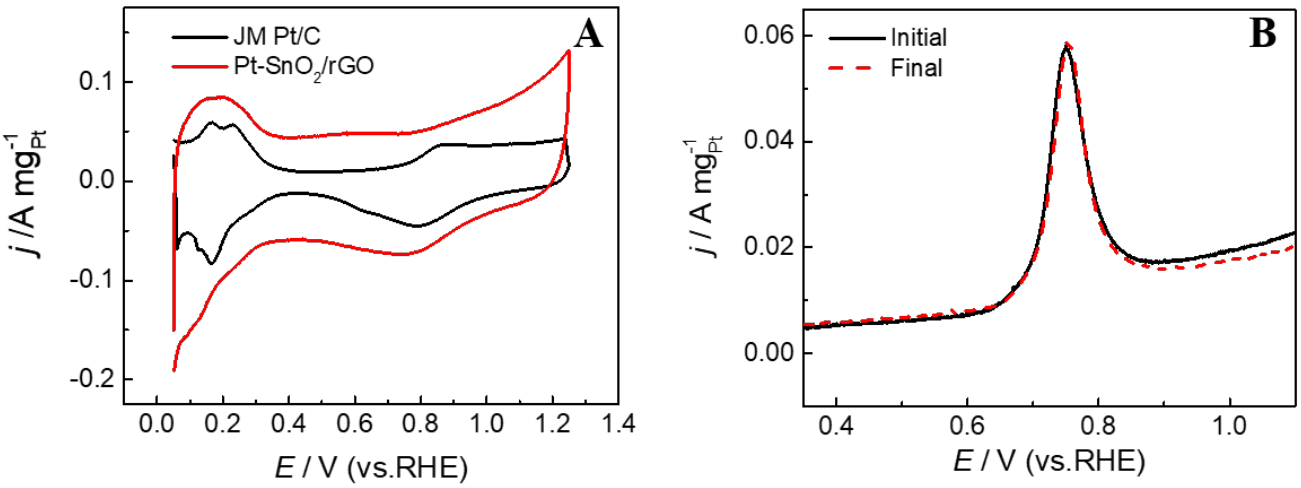

Figure S9. (A) CV curves of Pt-SnO_2/rGO and JM Pt/C in 1.0 M $HClO_4$ at a scan rate of 50 mV/s, (B) The CO stripping curves of Pt-SnO_2/rGO in 1.0 M $HClO_4$ before and after the chronoamperometric test.

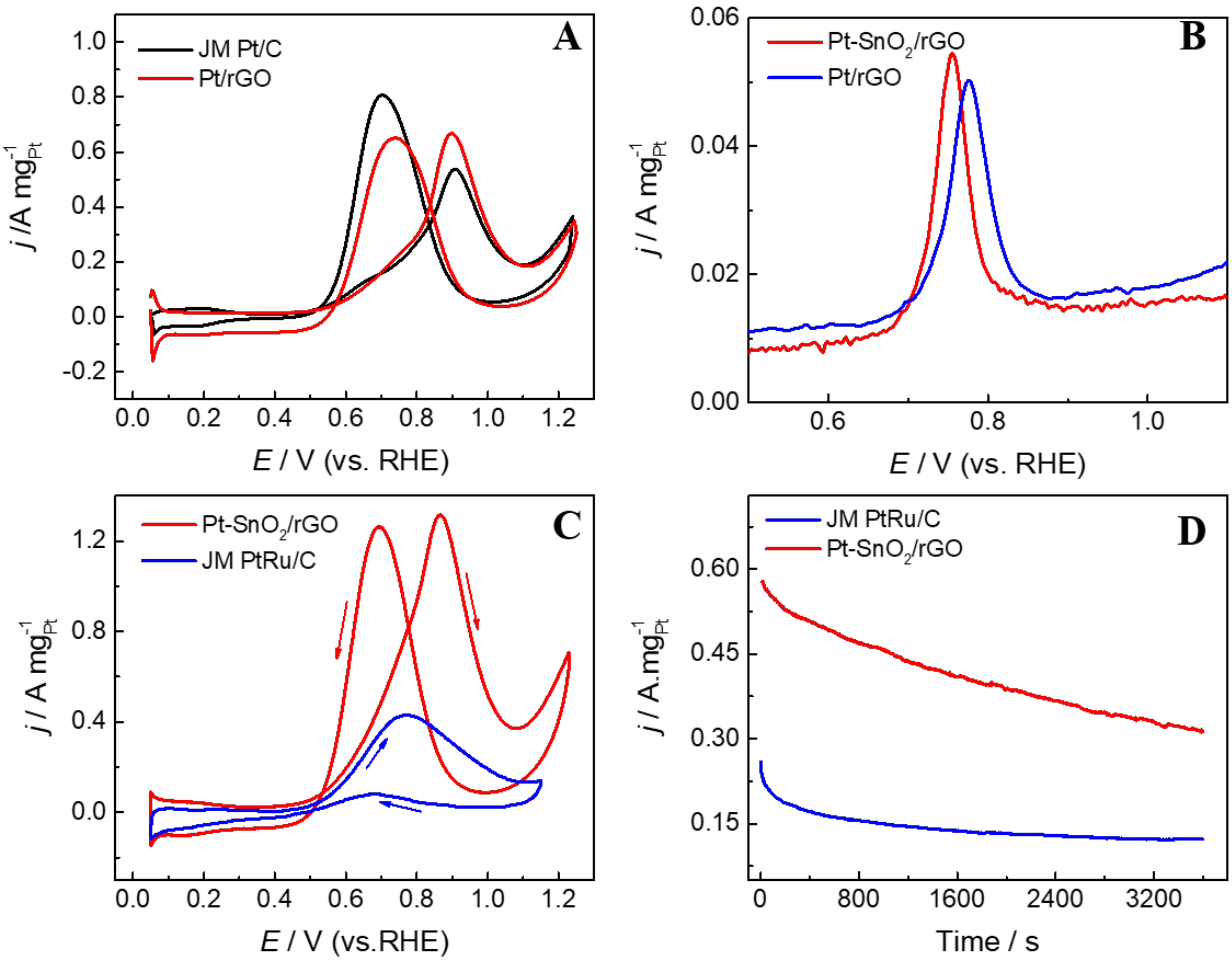

Figure S10. (A) Pt/rGO vs. JM Pt/C, CVs were recorded in 1 M $HClO_4$ + 1 M CH_3OH at a scan rate of 50 mV/s, (B) The CO stripping curves of Pt-SnO_2/rGO and Pt/rGO in 1.0 M $HClO_4$, (C) Pt-SnO_2/rGO vs. JM PtRu/C, CVs were recorded in 1 M $HClO_4$ + 1 M CH_3OH at a scan rate of 50 mV/s, (D) Chronoamperometric curves of Pt-SnO_2/rGO and JM PtRu/C recorded at 0.70 V (vs. RHE) in 1 M $HClO_4$ + 1 M CH_3OH.

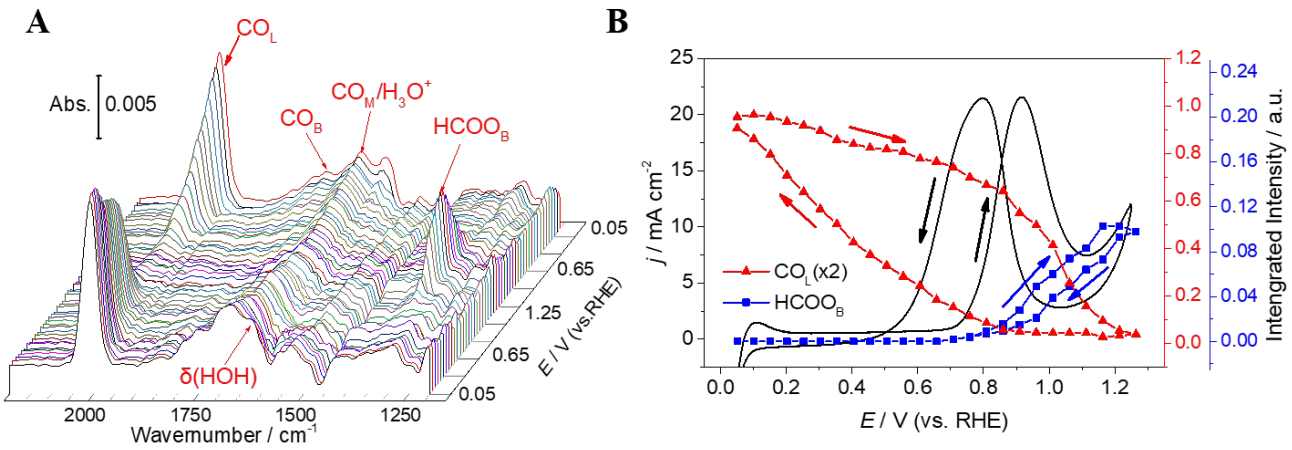

Figure S11. In situ ATR-SEIRAS spectra for (A) Pt/rGO in 1 M $HClO_4$ + 1 M CH_3OH with a time resolution of 5 s, using a single-beam spectrum at open circuit potential in 1 M $HClO_4$ as the reference spectrum, (B) Corresponding CVs of (C) Pt/rGO at a scan rate of 10 mV/s with the integrated band intensities of CO_L and $HCOO_B$. Current densities were normalized by geometric electrode area of 0.785 cm^2, and a constant catalyst loading was used for ATR-SEIRAS measurement, leading to an actual Pt mass loading of 0.55 mg_{Pt}/cm^2 for Pt/rGO.

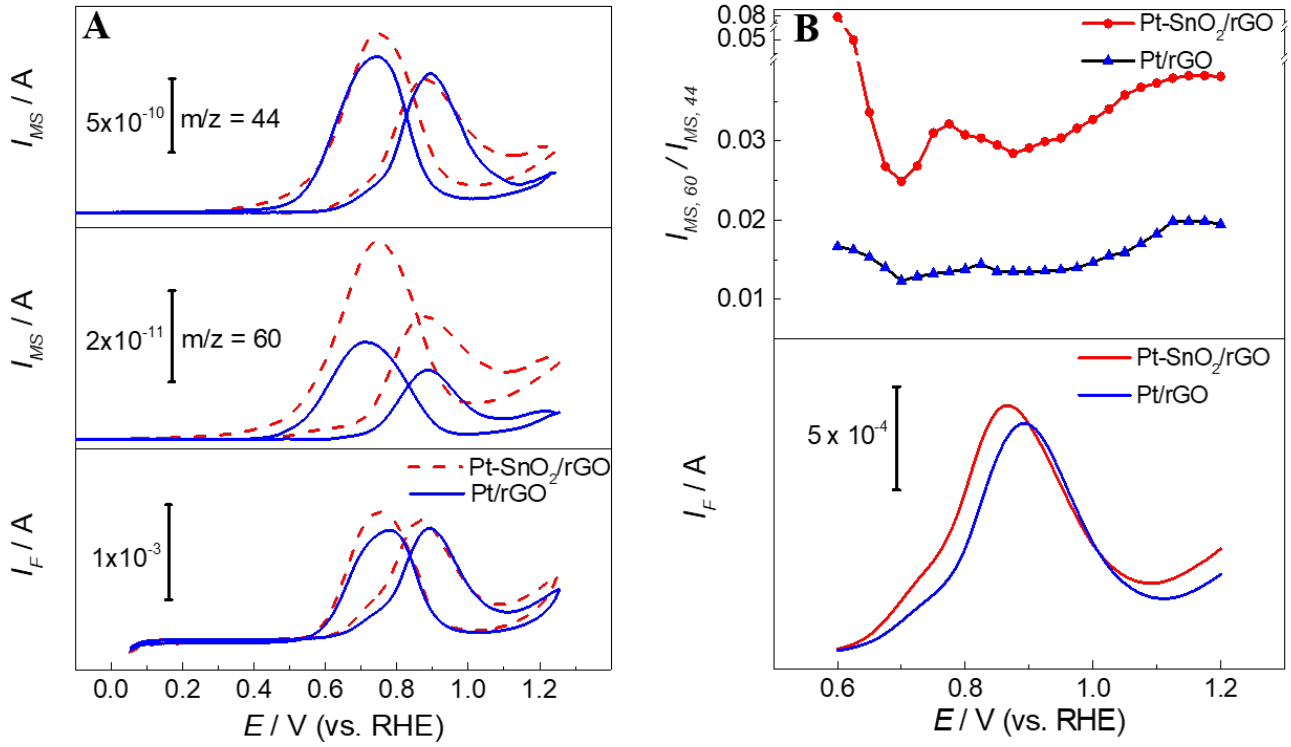

Figure S12. (A) Simultaneously recorded CVs and MSCVs for m/z = 44 and m/z = 60 on Pt/rGO and Pt-SnO_2/rGO in 1 M $HClO_4$ + 1 M CH_3OH at scan rate 5 mV/s; (B) the corresponding potential-dependent plot of the relative ratio $I_{MS,60}/I_{MS,44}$ as measured from 0.60 V to 1.20 V.

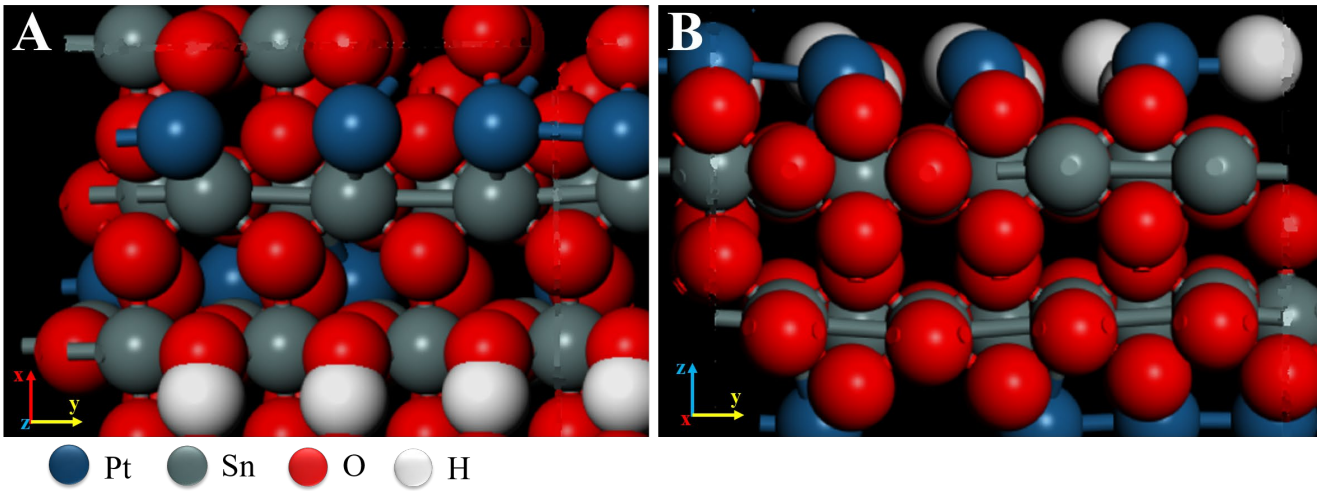

Figure S13. (A) Top view and (B) side view of the simulated Pt-SnO_2 structure.

Table S1. Pt L_3 edge EXAFS Fitting Results

Sample	Bond	CN	R / Å	σ^2 /(x10^{-3}Å^2)	ΔE / eV	R factor
Pt foil	Pt-Pt	12	2.75	-	-	-
JM Pt/C[a]	Pt-Pt	5.08±0.95	2.71±0.027	7.3	4.8	0.47%
	Pt-O	2.06±0.32	1.97±0.036	3.6	6.8	
SnO_2@Pt/rGO[b]	Pt-Pt	6.46±0.94	2.72±0.02	7.5	3.2	0.23%
	Pt-O	1.61±0.19	2.03±0.09	9.5	9.1	

[a] k-range = 3.349 - 13.808, [b] k-range = 3.226 – 12.449

Table S2. Comparison of MOR performances of Pt-SnO_2/rGO, other Pt-MO_x, and PtRu nanocatalysts from this work and recent published data.

Samples	Methanol concentration / M	Scan rate / $mV.s^{-1}$	Mass activity / $A.mg^{-1}$	Specific activity / $A.m^{-2}$	Peak Potential / V	Ref.
Pt-SnO_2/rGO	1.00	50	1.31	21.76	0.85 (vs.RHE)	This work
JM PtRu/C	1.00	50	0.43	4.32	0.79 (vs.RHE)	This work
Pt-CeO_2	0.50	50		27.5	0.90 (vs.RHE)	[1]
m-20Pt/WO3	0.50	50	0.59		0.72 (vs.Ag/AgCl)	[2]
7.5 wt% Pt/W2C	1.00	50	0.72	15.6	~0.86 (vs.Ag/AgCl)	[3]
Pt/$Ni(OH)_2$/rGO	1.00	50	1.07	15.0	-0.20 (vs.SCE)	[4]
PtSnO_2/C	1.00	20		0.50	0.84 (vs.NHE)	[5]
Fe_2O_3/Pt-b (Fe:Pt = 2:1)	1.00	50	1.26	22.10	0.18 (vs.MSE)	[6]
Pt-MoO_3/RGO (16.5% MoO_3)	0.50	50	0.61	5.65`	0.70 (vs.SCE)	[7]
Pt/RuO_2/CNTs	1.00	50	0.60	4.23	~0.75 (vs.Ag/AgCl)	[8]
Pt/TiO_2-C	1.00	50	0.42	5.76	~0.70 (vs.Ag/AgCl)	[9]
PtRu c-s	1.00	50	1.29	17.80	~0.75 (vs.RHE)	[10]
PtRu NWs /C	0.50	50	0.82	11.60	0.70 (vs.Ag/AgCl)	[11]
PtRu nanodenderites	1.00	50	1.08	27.00	~0.70 (vs.Ag/AgCl)	[12]
PtRu-CoP/C-40%	1.00	50	1.01	8.65	~0.53 (vs.SCE)	[13]

Table S3. IR Peak Assignments during MOR in this work

Wavernumber (cm^{-1})	Assignment
~1325	symmetric COO stretching mode of formate ($HCOO_B$)[14-17]
~1610	δ(HOH) of interfacial water[18, 19]
~1675	multi-bonded CO or interfacial hydronium[20]
1790 - 1900	Bridge-bonded CO band (CO_B)[20-22]
2010 - 2060	Linear-bonded CO band (CO_L)[20-22]

Table S4. Calculated reaction barriers (E_a, in eV) and reaction energies (ΔE, in eV) of the elementary steps in methanol dehydrogenation to surface CO* and formic acid over Pt-SnO_2

Surfaces	Pt-SnO_2	
Reactions	E_a	ΔE
$CH_3OH \rightarrow CH_3OH^*$	––	-0.97
$CH_3OH^* \rightarrow CH_3O^* + H^*$	0.34	-0.48
$CH_3O^* \rightarrow CH_2O^* + H^*$	0.33	-0.87
$CH_2O^* \rightarrow CHO^* + H^*$	0.44	-0.80
$CHO^* + OH^* \rightarrow HCOOH^*$	0.39	-0.49
$CHO^* \rightarrow CO^* + H^*$	0.62	-1.42

Table S5. Calculated reaction barriers (Ea, in eV) and reaction energies (ΔE, in eV) of the elementary steps in methanol dehydrogenation to surface CO* and formic acid over Pt (111)

Surfaces	Pt (111)	
Reactions	E_a	ΔE
$CH_3OH \rightarrow CH_3OH^*$	––	-0.28
$CH_3OH^* \rightarrow CH_2OH^* + H^*$	0.72	-0.11
$CH_2OH^* \rightarrow CHOH^* + H^*$	0.61	-0.17
$CHOH^* \rightarrow CHO^* + H^*$	0.60	0.04
$CHO^* + OH^* \rightarrow HCOOH^*$	0.49	-0.53
$CHO^* \rightarrow CO^* + H^*$	0.42	-0.98

Supplementary References

[1] Y.-Y. Chu, Z.-B. Wang, Z.-Z. Jiang, D.-M. Gu, G.-P. Yin, A Novel Structural Design of a Pt/C-CeO2 Catalyst with Improved Performance for Methanol Electro-Oxidation by beta-Cyclodextrin Carbonization, Adv. Mater., 23 (2011) 3100-3104.

[2] X. Cui, J. Shi, H. Chen, L. Zhang, L. Guo, J. Gao, J. Li, Platinum/mesoporous WO3 as a carbon-free electrocatalyst with enhanced electrochemical activity for methanol oxidation, J. Phys. Chem. B, 112 (2008) 12024-12031.

[3] R. Ganesan, J.S. Lee, Tungsten carbide microspheres as a noble-metal-economic electrocatalyst for methanol oxidation, Angew. Chem. Int. Ed., 44 (2005) 6557-6560.

[4] W. Huang, H. Wang, J. Zhou, J. Wang, P.N. Duchesne, D. Muir, P. Zhang, N. Han, F. Zhao, M. Zeng, J. Zhong, C. Jin, Y. Li, S.T. Lee, H. Dai, Highly active and durable methanol oxidation electrocatalyst based on the synergy of platinum-nickel hydroxide-graphene, Nat Commun, 6 (2015) 10035.

[5] A. Sandoval-González, E. Borja-Arco, J. Escalante, O. Jiménez-Sandoval, S.A. Gamboa, Methanol oxidation reaction on PtSnO 2 obtained by microwave-assisted chemical reduction, Int. J. Hydrogen Energy, 37 (2012) 1752-1759.

[6] Y.-T. Liu, Q.-B. Yuan, D.-H. Duan, Z.-L. Zhang, X.-G. Hao, G.-Q. Wei, S.-B. Liu, Electrochemical activity and stability of core–shell Fe 2 O 3 /Pt nanoparticles for methanol oxidation, J. Power Sources, 243 (2013) 622-629.

[7] Y. Hao, X. Wang, Y. Zheng, J. Shen, J. Yuan, A.-j. Wang, L. Niu, S. Huang, Uniform Pt Nanoparticles Incorporated into Reduced Graphene Oxides with MoO3 as Advanced Anode Catalysts for Methanol Electro-oxidation, Electrochim. Acta, 198 (2016) 127-134.

[8] F. Peng, C. Zhou, H. Wang, H. Yu, J. Liang, J. Yang, The role of RuO2 in the electrocatalytic oxidation of methanol for direct methanol fuel cell, Catal. Commun., 10 (2009) 533-537.

[9] Y.-H. Qin, Y. Li, R.-L. Lv, T.-L. Wang, W.-G. Wang, C.-W. Wang, Enhanced methanol oxidation activity and stability of Pt particles anchored on carbon-doped TiO 2 nanocoating support, J. Power Sources, 278 (2015) 639-644.

[10] S.T. Hunt, M. Milina, A.C. Alba-Rubio, C.H. Hendon, J.A. Dumesic, Y. Roman-Leshkov, Self-assembly of noble metal monolayers on transition metal carbide nanoparticle catalysts, Science, 352 (2016) 974-978.

[11] L. Huang, X. Zhang, Q. Wang, Y. Han, Y. Fang, S. Dong, Shape-Control of Pt-Ru Nanocrystals: Tuning Surface Structure for Enhanced Electrocatalytic Methanol Oxidation, J. Am. Chem. Soc., 140 (2018) 1142-1147.

[12] S. Lu, K. Eid, D. Ge, J. Guo, L. Wang, H. Wang, H. Gu, One-pot synthesis of PtRu nanodendrites as efficient catalysts for methanol oxidation reaction, Nanoscale, 9 (2017) 1033-1039.

[13] L. Feng, K. Li, J. Chang, C. Liu, W. Xing, Nanostructured PtRu/C catalyst promoted by CoP as an efficient and robust anode catalyst in direct methanol fuel cells, Nano Energy, 15 (2015) 462-469.
[14] Y.X. Chen, A. Miki, S. Ye, H. Sakai, M. Osawa, Formate, an active intermediate for direct oxidation of methanol on Pt electrode, J. Am. Chem. Soc., 125 (2003) 3680-3681.
[15] A. Miki, S. Ye, T. Senzaki, M. Osawa, Surface-enhanced infrared study of catalytic electrooxidation of formaldehyde, methyl formate, and dimethoxymethane on platinum electrodes in acidic solution, J. Electroanal. Chem., 563 (2004) 23-31.
[16] G. Samjeské, A. Miki, S. Ye, M. Osawa, Mechanistic Study of Electrocatalytic Oxidation of Formic Acid at Platinum in Acidic Solution by Time-Resolved Surface-Enhanced Infrared Absorption Spectroscopy, J. Phys. Chem. B, 110 (2006) 16559-16566.
[17] A. Miki, S. Ye, M. Osawa, Surface-enhanced IR absorption on platinum nanoparticles: an application to real-time monitoring of electrocatalytic reactions, Chem. Commun., (2002) 1500-1501.
[18] T. Iwasita, Electrocatalysis of methanol oxidation, Electrochim. Acta, 47 (2002) 3663-3674.
[19] E.A. Batista, G.R.P. Malpass, A.J. Motheo, T. Iwasita, New mechanistic aspects of methanol oxidation, J. Electroanal. Chem., 571 (2004) 273-282.
[20] E.A. Batista, T. Iwasita, W. Vielstich, Mechanism of stationary bulk CO oxidation on Pt(111) electrodes, J. Phys. Chem. B, 108 (2004) 14216-14222.
[21] S.X. Liu, L.W. Liao, Q. Tao, Y.X. Chen, S. Ye, The kinetics of CO pathway in methanol oxidation at Pt electrodes, a quantitative study by ATR-FTIR spectroscopy, Phys. Chem. Chem. Phys., 13 (2011) 9725-9735.
[22] W.F. Lin, M.S. Zei, M. Eiswirth, G. Ertl, T. Iwasita, W. Vielstich, Electrocatalytic activity of Ru-modified Pt(111) electrodes toward CO oxidation, J. Phys. Chem. B, 103 (1999) 6968-6977.